Failure of a Glass Ionomer to Remineralize Apatite-depleted Dentin

Y.K. Kim, C.K.Y. Yiu, J.R. Kim, L. Gu, S.K. Kim, R.N. Weller, D.H. Pashley and F.R. Tay

J DENT RES 2010 89: 230 originally published online 28 January 2010
DOI: 10.1177/0022034509357172

RESEARCH REPORTS
Biomaterials & Bioengineering

Y.K. Kim[1], C.K.Y. Yiu[2], J.R. Kim[3], L. Gu[4], S.K. Kim[1], R.N. Weller[5], D.H. Pashley[6], and F.R. Tay[5,6]*

[1]Department of Conservative Dentistry, School of Dentistry, Kyungpook National University, Daegu, Korea; [2]Pediatric Dentistry & Orthodontics, Faculty of Dentistry, University of Hong Kong, Hong Kong SAR, China; [3]Department of Conservative Dentistry, School of Dentistry, KyungHee University, Seoul, Korea; [4]Department of Operative Dentistry and Endodontics, Guanghua School of Stomatology, Sun Yat-sen University, Guangzhou, China; [5]Department of Endodontics, School of Dentistry, Medical College of Georgia, Augusta, GA 30912-1129, USA; and [6]Department of Oral Biology, School of Dentistry, Medical College of Georgia, Augusta, GA, USA; *corresponding author, ftay@mcg.edu

J Dent Res 89(3):230-235, 2010

Failure of a Glass Ionomer to Remineralize Apatite-depleted Dentin

ABSTRACT

Remineralization of demineralized dentin lesions adjacent to glass-ionomer cements (GICs) has been reported in the literature. This study tested the hypothesis that a strontium-based GIC can remineralize completely demineralized dentin by nucleation of new apatite crystallites within an apatite-free dentin matrix. Human dentin specimens were acid-etched, bonded with Fuji IX_{GP}, and immersed in a calcium-and-phosphate-containing 1.5X simulated body fluid (SBF) for 1-4 months. Polyacrylic acid and polyvinylphosphonic acid biomimetic analogs were added to the SBFs to create 2 additional remineralization media. Specimens were processed by transmission electron microscopy (TEM). No apatite deposition could be identified in the completely demineralized dentin in any of the specimens immersed in the 3 remineralization media, despite TEM/EDX evidence of diffusion of ions specific to the strontium-based GIC into the demineralized dentin. The hypothesis was rejected; mineral concentration alone is not a sufficient endpoint for assessing the success of contemporary remineralization strategies.

KEY WORDS: glass-ionomer cement, demineralized dentin, remineralization, apatite, ion diffusion.

DOI: 10.1177/0022034509357172

Received March 10, 2009; Last revision September 3, 2009; Accepted September 25, 2009

INTRODUCTION

Glass-ionomer cements (GICs) have been widely used in restorative dentistry (Mount, 1998), due to their self-adhesive and fluoride-releasing properties (Naasan and Watson, 1998). Indirect evidence of the ability of GICs to remineralize artificial caries lesions was based on the results of microradiography and micro-computed tomography (Creanor *et al.*, 1998; Exterkate *et al.*, 2005; Lee *et al.*, 2008). The use of energy-dispersive x-ray microanalysis (EDS) (Massara *et al.*, 2002) and electron probe microanalysis (EPMS) (Kitasako *et al.*, 2003; Ab-Ghani *et al.*, 2007) further revealed changes in mineral profiles of specific elements across the GIC-tooth interface. Despite evidence of ion exchange between GICs and dentin at a chemical level (Coutinho *et al*., 2007), there is no direct ultrastructural evidence of interfibrillar or intrafibrillar remineralization of the demineralized collagen matrix. Intrafibrillar remineralization, in particular, is crucial for restoring the mechanical properties of partially mineralized dentin to those of mineralized dentin (Kinney *et al*., 2003).

A recent report presented a successful strategy for *in situ* remineralization of phosphoric-acid-etched dentin in the presence of biomimetic analogs (Tay and Pashley, 2008). In that study, transmission electron microscopy (TEM) and electron diffraction were used to establish definitive evidence of interfibrillar and intrafibrillar apatite deposition within the collagen fibrils of the demineralized dentin matrix. These ultrastructural techniques were indispensible in discriminating the dimensions and ordered arrangement of apatite platelets in mineralized tissues (Traub *et al*., 1989). Incorporation of biomimetic analogs of non-collagenous proteins into the remineralization medium helped to stabilize amorphous calcium phosphate precursors in their nanoscale dimensions (Zhang and Webster, 2009). The analogs further served as templates that guided the self-assembly of the stabilized nanoprecursors along specific sites of the collagen fibrils (Gajjeraman *et al.*, 2007), their subsequent transformation into nanoapatites, and fusion into conventional apatite crystallites. These phenomena were thought to proceed *via* the non-classic crystallization pathways of "bottom-up" nanoparticle assembly and mesocrystalline transformation (Niederberger and Cölfen, 2006).

Fuji IX_{GP} (GC International, Tokyo, Japan) is a strontium-based GIC developed for the Atraumatic Restorative Treatment of carious dentin (Massara *et al.*, 2002; Amaral *et al.*, 2006). It has been demonstrated that ions specific to Fuji IX_{GP} penetrated deeply into caries-affected dentin (Ngo *et al.,* 2006). Those

authors considered the presence of strontium and aluminum ions in the demineralized dentin matrix as evidence of a remineralization process. In this study, we challenged the ability of Fuji IX_{GP} to remineralize completely demineralized dentin at an ultrastructural level by testing the hypothesis that the strontium-based GIC can successfully remineralize completely demineralized dentin by nucleation of new apatite crystallites within an apatite-free dentin matrix.

MATERIALS & METHODS

Specimen Preparation

Twenty-one non-carious human third molars were collected after donors' informed consents were obtained under a protocol approved by the Human Assurance Committee of the Medical College of Georgia. For each tooth, a flat surface was created in mid-coronal dentin by means of a slow-speed Isomet diamond saw (Buehler Ltd, Lake Bluff, IL, USA) under water cooling. The surface was polished with 600-grit silicon carbide paper under running water. A second parallel cut was made at the cemento-enamel junction to create a dentin block that was devoid of pulpal tissues.

Placement of GIC

Each coronal dentin surface was etched with 32% phosphoric acid gel (Bisco Inc., Schaumburg, IL, USA) for 1 min to create a completely demineralized dentin layer on top of a mineralized dentin base. The etched surface was rinsed with de-ionized water and covered with moistened lint-free tissues to prevent desiccation of the demineralized collagen matrix.

Fuji IX_{GP} capsules were triturated for 10 sec and dispensed over the acid-etched dentin to produce 5-mm-thick cores, resulting in 16 GIC-bonded specimens. After initial setting, the exposed GICs were coated with nail varnish, leaving only the dentinal tubules along the pulpal side of the dentin blocks as pathways of communication between the remineralization media and the bonded dentin (Czarnecka *et al.*, 2002). After storage at 37°C and 100% relative humidity for 24 hrs, the bonded specimens were immersed in the designated remineralization medium. One of the Fuji IX_{GP} specimens was not immersed in any of the 3 remineralization media, but was analyzed as a 24-hour baseline specimen.

Remineralization Media

We prepared a 1.5X simulated body fluid (SBF; Kokubo and Takadama, 2006) by dissolving 205.2 mM NaCl, 6.3 mM $NaHCO_3$, 4.5 mM KCl, 1.5 mM $K_2HPO_4{\cdot}3H_2O$, 2.25 mM $MgCl_2{\cdot}6H_2O$, 3.75 mM $CaCl_2$, and 0.75 mM Na_2SO_4 in de-ionized water and adding 3.08 mM sodium azide to prevent bacterial growth. This 1.5X SBF served as the classic remineralization medium, which contained no biomimetic analog. Two additional biomimetic remineralization media were prepared. For the first medium, 200-800 μg/mL of polyvinylphosphonic acid (PVPA; Sigma-Aldrich, St. Louis, MO, USA) was added to the 1.5X SBF as the sole biomimetic analog. Polyacrylic acid (PAA), being a component of the GIC liquid, was not used in this medium. For the other medium, the 1.5X SBF was supplemented with 200-800 μg/mL of PVPA and 200-1,500 μg/mL of PAA (MW 1,800; Sigma-Aldrich) as dual biomimetic analogs. All solutions were buffered to pH 7.2 with 0.1 M Tris Base or 0.1 M HCl.

Remineralization of GIC-bonded Dentin

The GIC-bonded dentin specimens were randomly divided into 3 groups (N = 5) according to the remineralization medium. Each specimen was placed in a glass scintillation vial that was filled with 15 mL of the respective medium. The medium was changed every mo. Specimens were retrieved after 1-4 mos for ultrastructural examination of the extent of remineralization. Each specimen was sectioned occluso-gingivally into a 0.9-mm-thick slab containing the GIC-dentin interface after 1, 2, 3, or 4 mos. The exposed GIC-dentin interface of the intact specimen was protected with nail varnish after being sectioned. The assembly was returned to the vial for continuous remineralization prior to being re-sectioned at the second, third, and fourth mos.

Portland Cement-based Biomimetic Remineralization Control

The remaining 5 teeth were subjected to a biomimetic remineralization scheme that was slightly modified from the one reported previously (Tay and Pashley, 2008). Briefly, white Portland cement was mixed at a water-to-powder ratio of 0.35:1, and placed on top of an unetched dentin disk with a piece of Saran wrap placed between the dentin surface and the cement to obtain an impression of the dentin disk. After the mixture set, the Saran wrap was removed. The dentin surface was etched with 32% phosphoric acid for 60 sec. The set cement block was placed over the acid-etched dentin, and the assembly was immersed in 15 mL of the aforementioned second biomimetic remineralization medium (1.5X SBF with dual biomimetic analogs PAA and PVPA). Monthly sectioning of the specimen slabs followed the manner described for the GIC specimens, with the exception that the Portland cement-dentin assemblies were stabilized with sewing threads prior to being sectioned. The exposed interfaces were protected with varnish.

Transmission Electron Microscopy

The specimen slabs were prepared for TEM according to a previously reported protocol (Tay and Pashley, 2008). Briefly, the specimens were dehydrated in ethanol (70-100%), immersed in propylene oxide, and embedded in epoxy resin. Non-demineralized, 90- to 110-nm-thick sections were prepared and examined unstained in a JEM-1230 TEM (JEOL, Tokyo, Japan) operated at 110 kV. Selected area electron diffractions (SAEDs) were performed at specific locations of the TEM sections, with centered dark-field imaging.

Elemental Distribution

Representative 4-month-old specimens from the 3 GIC remineralization groups were examined by TEM-EDS in a Tecnai G2-20 TEM equipped with a scanning transmission attachment (FEI Co., Hillsboro, OR, USA). Line scans were performed for the distribution of calcium, phosphorus, strontium, aluminum, and fluorine across the GIC-dentin interfaces.

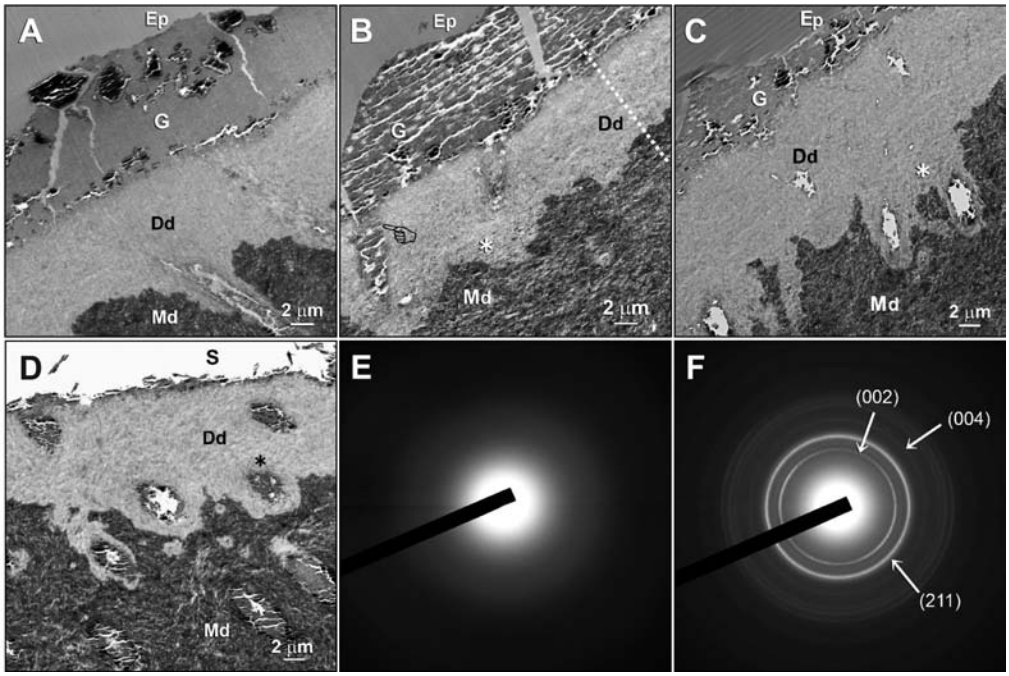

Figure 1. Transmission electron micrographs (TEMs) and selected area electron diffraction (SAED) taken from unstained, non-demineralized sections of glass-ionomer cement (GIC)-dentin interfaces. (**A)** A 24-hour baseline specimen that had not been immersed in any of the 3 remineralization media. A layer of apatite-depleted, completely demineralized dentin was produced by 60 sec of phosphoric-acid-etching. Desiccation artifacts could be seen within the GIC. (**B)** Low-magnification view of a representative specimen that had been immersed in a simulated body fluid (SBF) devoid of biomimetic analogs for 4 mos. The GIC formed tags (pointer) within the dentinal tubules. A zone of demineralized dentin containing electron-dense grains (Ed) was seen above the mineralized dentin base (asterisk). (**C)** A representative specimen that had been immersed in a polyvinylphosphonic acid (PVPA)-containing SBF for 4 mos. A basal Ed zone (asterisk) could be seen adjacent to the mineralized dentin base. (**D)** A representative specimen that had been immersed in a polyacrylic acid- and PVPA-containing SBF for 4 mos. The epoxy-resin-embedded GIC dislodged during sectioning, leaving a space (S) on top of the GIC remnants. Sectioning artifacts could be observed within the GIC glass particles. The Ed appeared diffuse throughout the demineralized dentin, although they were more concentrated around the periphery of dentinal tubules (asterisk). (**E)** A SAED pattern that is representative of the Ed-containing demineralized dentin. The diffuse electron diffraction pattern was indicative of the absence of crystalline phases within the demineralized dentin. (**F)** SAED collected from the mineralized dentin base revealed discrete rings indicative of the polycrystalline nature of the mineral phases. The indices confirmed the presence of apatites within the naturally mineralized dentin. Generic abbreviations: Ep, epoxy resin; G, GIC; Dd, demineralized dentin; Md, mineralized dentin.

RESULTS

The baseline specimen revealed an 8- to 12-µm-thick layer of completely demineralized dentin created by 60 sec of phosphoric-acid-etching. The GIC adapted well to the apatite-depleted dentin surface (Fig. 1A). Apatite re-deposition was not apparent within the demineralized dentin matrices of any of the 1- to 4-month-old GIC-restored specimens, regardless of their medium type and immersion times. Nevertheless, a zone of electron-dense grains (Ed) containing demineralized dentin was identified adjacent to the mineralized dentin base after the specimens were immersed in the 3 remineralization media (Figs. 1B-1D, 2B). Diffuse SAED patterns derived from the Ed-containing demineralized dentin (Fig. 1E) indicated the absence of crystalline phases within these regions. By contrast, SAED ring patterns collected from the mineralized dentin base were characteristic of polycrystalline apatite (Fig. 1F).

Higher-magnification views of the unstained, Ed-containing demineralized dentin revealed excellent banding characteristics and the rope-like subfibrillar architecture of the collagen fibrils (Figs. 2A, 2D). Although interfibrillar spaces and the terminal branches of dentinal tubules were highlighted by an apparent negative staining effect (Figs. 2C, 2E), intrafibrillar and interfibrillar mineral crystallites were absent throughout the collagen matrix.

Elemental distributions across the GIC-dentin interface from a representative specimen that had been immersed in 1.5X SBF for 4 mos are shown in Fig. 3. Fuji IX_{GP}-specific elements (aluminum and strontium) and fluorine were present in the demineralized dentin layer. These elements had intensity levels similar to or slight lower than those present in the GIC material. Compared with mineralized dentin, calcium and phosphorus intensity levels were lower in the demineralized dentin layer. Similar results were seen in specimens retrieved from the other 2 remineralization media (not shown).

For the Portland cement control, specimens that were immersed in PAA- and PVPA-containing remineralization medium exhibited foci of remineralization within the demineralized dentin matrix at 2 mos (Fig. 4A). Coalescence of these foci resulted in heavier, but incomplete, remineralization along the entire thickness of the matrix at 3 (Fig. 4C) and 4 mos (Fig. 4D). There was clear evidence of intrafibrillar remineralization within the collagen fibrils (Figs. 4B,4E).

DISCUSSION

In the present study, we used a model consisting of an 8- to 12-µm-thick layer of completely demineralized dentin to evaluate the status of remineralization. This model is different from the more conventionally used artificial caries model that consists of 200- to 300-µm-thick layers of partially demineralized dentin (ten Cate, 2001). Both models have inherent flaws, in that they do not simulate the tubular occlusion characteristics of caries-affected dentin (Zavgorodniy *et al.*, 2008). From a thickness perspective, the

former model is less taxing, in that one is unlikely to be able to remineralize a thick caries lesion if one could not even remineralize a demineralized dentin layer that is 1/20-1/30 its thickness. The former model is more challenging from a thermodynamic perspective, since it would have been easier to remineralize partially demineralized dentin that contains remnant apatite seed crystallites (Liu *et al*., 1997) for epitaxial growth (*i.e*., heterogeneous nucleation). Conversely, remineralization of a completely demineralized collagen matrix *via* a homogeneous nucleation mechanism is more thermodynamically and kinetically demanding (Wang and Nancollas, 2009). Nevertheless, the major reason for adopting the completely demineralized dentin model was to eliminate the ambiguity in differentiating partially demineralized apatite seed crystallites from remineralized apatite crystallites. This procedure is virtually impossible, even at the ultrastructural level, without resorting to high-precision chemo-analytical techniques for bulk analysis of ion-substituted apatites (Pietak *et al*., 2007).

The Fuji IX_{GP} adapted well to the completely demineralized dentin. Glass particles within the polyalkenoate matrices were enclosed within a hydrogel layer indicative of a GI reaction. It is generally accepted that GICs bond chemically to tooth substrates through ionic bonds with calcium ions of apatite (Mount, 1991; Lin *et al*., 1992). This chemical bonding was confirmed by x-ray photoelectron spectroscopy (Yoshida *et al*., 2000). The present study provided evidence that GICs adapted well to apatite-depleted dentin surfaces.

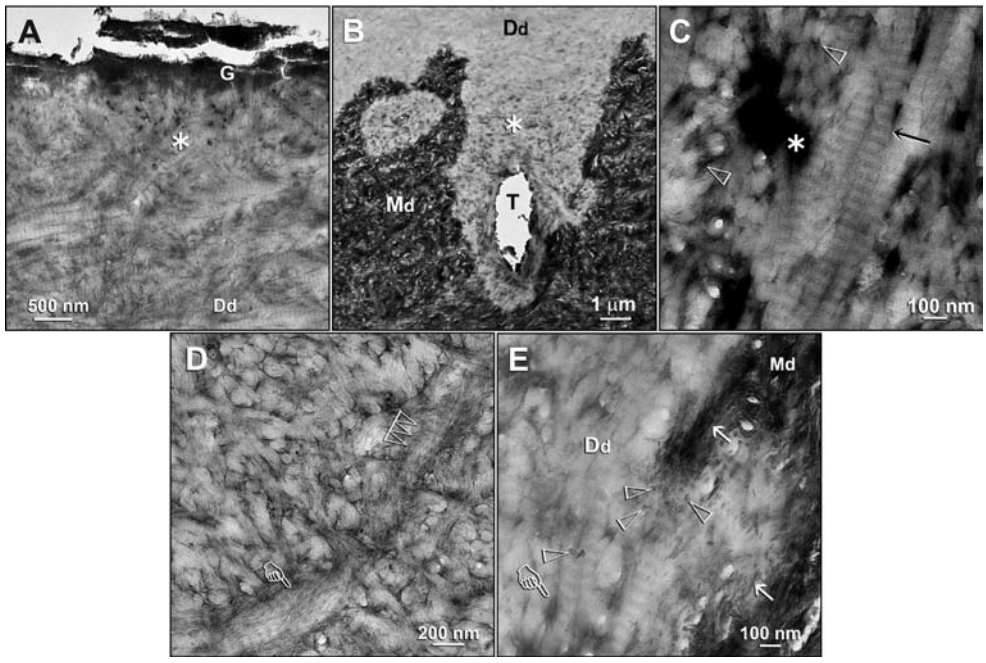

Figure 2. Ultrastructural characterization of the electron-dense grains (Ed)-containing zones in the demineralized dentin layers derived from specimens that had been immersed in the remineralization media. (**A)** A specimen that had been immersed in a PVPA-containing SBF for 4 mos. The electron-dense grainy materials were not exclusively found along the base of the demineralized dentin layer. A higher-magnification view of the junction between the fractured GIC (G) and the underlying demineralized dentin surface revealed an Ed-containing superficial region (asterisk). Although no additional staining was used, excellent banding characteristics of the demineralized dentin collagen matrix (Dd) could be observed. (**B)** An Ed-containing zone (asterisk) at the base of the demineralized dentin layer. The specimen had been immersed in a polyacrylic acid- and PVPA-containing SBF for 4 mos. T: dentinal tubule. (**C)** A high-magnification view of the Ed-containing regions depicted by the "asterisk" in Figs. 2A and 2B revealed a strong negative staining effect, in this bright-field micrograph, that was created in the absence of the use of an extrinsic negative stain. Banding could be identified within the collagen fibrils (arrow) even in the absence of extrinsic staining. No mineral crystallites could be identified around or within these fibrils. Open arrowheads: interfibrillar spaces between the collagen fibrils. (**D)** A high-magnification view of the area labeled with "Dd" in Fig. 2A. Dark interfibrillar spaces were present despite the absence of the larger, dark terminal tubular channels seen in Fig. 2C. Apart from banding of the collagen fibrils (multiple open arrowheads), the rope-like subfibrillar architecture of the collagen fibril (pointer) was highlighted by the negative staining. No intrafibrillar or interfibrillar crystallites could be identified in these fibrils. (**E)** A high-magnification view of the junction between the Ed-containing zone and the mineralized dentin base in Fig. 2B. Remnants of apatite platelets (open arrowheads) and needles (arrows) were present along the demineralization front. The Ed within the interfibrillar spaces and terminal tubular branches (pointer) appeared less electron-dense, due to the auto-contrast function of the microscope in the presence of the highly mineralized dentin base along the right side of the micrograph. The absence of apatite remineralization in the negatively stained collagen fibrils and the adjacent interfibrillar spaces is clearly evident. Generic abbreviations: Dd, demineralized dentin; Md, mineralized dentin.

The collagen banding and rope-like subfibrillar features identified in unstained bright-field TEM micrographs of the aged-Fuji IX_{GP} specimens represent an unusual self-generated negative staining phenomenon. Penetration of Fuji IX_{GP}-specific mineral ions (aluminum or strontium) into the collagen matrix probably accounted for the negative staining of the collagen fibrils. Although salts of heavy metals such as molybdenum, tungsten, and uranium have been conventionally used as negative stains, the salts of certain lighter metals, such as sodium, magnesium, and aluminum, may also be used for similar purposes (Massover, 2008). Electron-dense grainy regions were universally identified, but were more prominently seen along the base of the demineralized dentin. Presumably, the collagen fibrils and terminal branches of the dentinal tubules at these locations were less collapsed than those that are more superficially located, facilitating better infiltration of the mineral ions.

In Fuji IX_{GP}, conventional calcium glass powder is substituted by a strontium-based glass to enhance its radiopacity. Strontium is similar to calcium in both chemical and physical properties, so that it can replace calcium without disrupting the apatite structure. Moreover, strontium has been perceived to play a pivotal role in

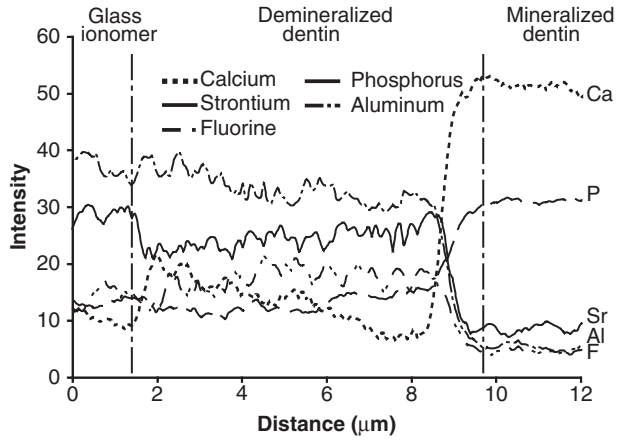

Figure 3. TEM-EDS line scans of the distribution of calcium (Ca), phosphorus (P), aluminum (Al), strontium (Sr), and fluorine (F) across a representative GIC-dentin interface in a specimen that had been immersed in the SBF devoid of biomimetic analogs for 4 mos. The white dotted line in Fig. 1B represents the generic location upon which elemental analyses were performed across the GIC-dentin interfaces. The changes in elemental profiles may be divided into 3 distinct zones, beginning at the left: **(A)** In the GIC restoration, strontium, aluminum, and fluorine intensity levels were higher than those in the sound dentin; **(B)** within the demineralized dentin layer, the 2 GIC-specific elements (strontium, aluminum) were similar to and slightly lower than their corresponding levels in the GIC proper, while, conversely, calcium and phosphorus intensities were low within this demineralized layer; and **(C)** within the mineralized dentin base, the intensity levels of the 2 GIC-specific elements and fluorine decreased to their lowest levels, while those of calcium and phosphorus increased to their maximum levels.

chemical bond formation with tooth apatite (Wilson *et al.*, 1983). In the present study, diffusion of strontium, aluminum, and fluorine ions into the completely demineralized dentin matrix was consistent with previously reported findings (Ngo *et al.*, 2006) on partially demineralized caries-affected dentin. Diffusion of GIC-specific ions into the demineralized dentin probably occurs as a result of the ion concentration gradient that exists between GICs and dentin (Ferrari and Davidson, 1997; Knight *et al.*, 2007).

The contributions of non-collagenous proteins to dentin remineralization had seldom been considered in classic remineralization studies, except by a few authors (Clarkson *et al.*, 1998; Saito *et al.*, 2003). It is well-known in biomineralization that non-collagenous proteins or their biomimetic analogs are required for generating apatites of the dimensions and order that can fit into the gap zones of type I collagen fibrils. The results of this study indicated that, apart from the uptake of GIC-specific ions, there was no ultrastructural evidence of mineral deposition of a crystalline nature in the Fuji IX_{GP}-bonded acid-etched, completely demineralized dentin, regardless of whether a classic (non-biomimetic) or a biomimetic remineralization strategy (single- or dual-biomimetic analogs) was utilized. Moreover, microradiography-demonstrated reduction of lesion size in "remineralized" artificial carious dentin (Ten Bosch and Angmar-Månsson, 1991) does not imply that the radiopaque mineral precipitates are small enough to permit carbonated apatite to form inside and around collagen fibrils in demineralized dentin. Indeed, the instrumentation and resolutions used in some combined microradiography/morphologic studies on dentin remineralization (Kawasaki *et al.*, 1999) were insufficient to permit such an intricate relation to be determined.

Based on the results of the Portland cement-based biomimetic remineralization control, we have to reject the hypothesis that a strontium-based GIC can remineralize completely demineralized dentin by nucleation of new apatite crystallites within an apatite-free dentin matrix. It is premature to extrapolate the results of the present study to caries-affected partially demineralized dentin, since the latter contains remaining apatite crystals which may constitute centers for heterogeneous nucleation (thus requiring less thermodynamic drive) and remineralization (which possibly involves epitaxial growth mechanisms of remaining crystals). Nevertheless, this study raises the issue of the possibility of non-remineralization of a dentin caries lesion that may contain apatite-depleted collagen matrices along the surface of the lesion. The results of the present study support the challenge raised (Kinney *et al.*, 2003) to classic remineralization studies, that the use of mineral uptake alone is not a sufficient endpoint for assessing the success of contemporary remineralization strategies.

ACKNOWLEDGMENTS

The Fuji IX_{GP} capsule kits were generous gifts from GC America, Inc. This study was supported by Grant R21 DE019213-01 from the National Institute of Dental and Craniofacial Research (PI. F.R. Tay). We thank Bob Smith for TEM technical assistance and Michelle Barnes for secretarial support.

REFERENCES

Ab-Ghani Z, Ngo H, McIntyre J (2007). Effect of remineralization/demineralization cycles on mineral profiles of Fuji IX Fast *in vitro* using electron probe microanalysis. *Aust Dent J* 52:276-281.

Amaral MT, Guedes-Pinto AC, Chevitarese O (2006). Effects of a glass-ionomer cement on the remineralization of occlusal caries - an *in situ* study. *Braz Oral Res* 20:91-96.

Clarkson BH, Chang SR, Holland GR (1998). Phosphoprotein analysis of sequential extracts of human dentin and the determination of the subsequent remineralization potential of these dentin matrices. *Caries Res* 32:357-364.

Coutinho E, Yoshida Y, Inoue S, Fukuda R, Snauwaert J, Nakayama Y, *et al*. (2007). Gel phase formation at resin-modified glass-ionomer/tooth interfaces. *J Dent Res* 86:656-661.

Creanor SL, Awawdeh LA, Saunders WP, Foye RH, Gilmour WH (1998). The effect of a resin-modified glass ionomer restorative material on artificially demineralised dentine caries *in vitro*. *J Dent* 26:527-531.

Czarnecka B, Limanowska-Shaw H, Nicholson JW (2002). Buffering and ion-release by a glass-ionomer cement under near-neutral and acidic conditions. *Biomaterials* 23:2783-2788.

Exterkate RA, Damen JJ, ten Cate JM (2005). Effect of fluoride-releasing filling materials on underlying dentinal lesions *in vitro*. *Caries Res* 39:509-513.

Ferrari M, Davidson CL (1997). Interdiffusion of a traditional glass ionomer cement into conditioned dentin. *Am J Dent* 10:295-297; erratum in *Am J Dent* 11:28, 1998.

Gajjeraman S, Narayanan K, Hao J, Qin C, George A (2007). Matrix macromolecules in hard tissues control the nucleation and hierarchical assembly of hydroxyapatite. *J Biol Chem* 282:1193-1204.

Kawasaki K, Ruben J, Stokroos I, Takagi O, Arends J (1999). The remineralization of EDTA-treated human dentine. *Caries Res* 33:275-280.

Kinney JH, Habelitz S, Marshall SJ, Marshall GW (2003). The importance of intrafibrillar mineralization of collagen on the mechanical properties of dentin. *J Dent Res* 82:957-961.

Kitasako Y, Nakajima M, Foxton RM, Aoki K, Pereira PN, Tagami J (2003). Physiological remineralization of artificially demineralized dentin beneath glass ionomer cements with and without bacterial contamination *in vivo*. *Oper Dent* 28:274-280.

Knight GM, McIntyre JM, Craig GG, Mulyani (2007). Electron probe microanalysis of ion exchange of selected elements between dentine and adhesive restorative materials. *Aust Dent J* 52:128-132.

Kokubo T, Takadama H (2006). How useful is SBF in predicting *in vivo* bone bioactivity? *Biomaterials* 27:2907-2915.

Lee HS, Berg JH, Garcia-Godoy F, Jang KT (2008). Long-term evaluation of the remineralization of interproximal caries-like lesions adjacent to glass-ionomer restorations: a micro-CT study. *Am J Dent* 21:129-132.

Lin A, McIntyre NS, Davidson RD (1992). Studies on the adhesion of glass-ionomer cements to dentin. *J Dent Res* 71:1836-1841.

Liu Y, Sethuraman G, Wu W, Nancollas GH, Grynpas M (1997). The crystallization of fluorapatite in the presence of hydroxyapatite seeds and of hydroxyapatite in the presence of fluorapatite seeds. *J Colloid Interface Sci* 186:102-109.

Massara ML, Alves JB, Brandão PR (2002). Atraumatic restorative treatment: clinical, ultrastructural and chemical analysis. *Caries Res* 36:430-436.

Massover WH (2008). On the experimental use of light metal salts for negative staining. *Microsc Microanal* 14:126-137.

Mount GJ (1991). Adhesion of glass-ionomer cement in the clinical environment. *Oper Dent* 16:141-148.

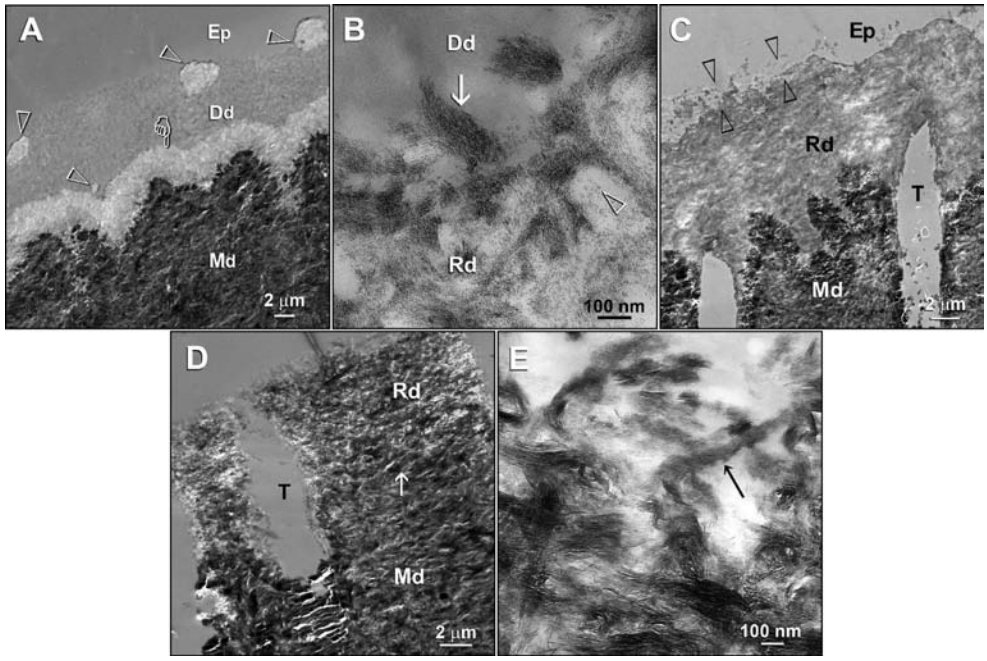

Figure 4. TEMs taken from unstained, non-demineralized sections of acid-etched dentin in the Portland cement-based biomimetic remineralization control group. (**A)** A specimen retrieved after 2 mos of biomimetic remineralization in the polyacrylic acid- and PVPA-containing SBF revealed discrete islands of partial remineralization (open arrowheads) and a 3-μm-thick zone of partial remineralization (pointer) over the original demineralization front. (**B)** A high-magnification view of partially remineralized dentin depicted in Fig. 4A. Collagen fibrils along the dentin surface (arrow) were heavily remineralized with nanocrystals. Individual nanocrystals (open arrowhead) could also be seen in the less-highly-remineralized regions. (**C)** A 3-month-old specimen retrieved from the polyacrylic acid- and PVPA-containing SBF revealed heavier remineralization than extended from the dentin surface to the mineralized dentin base. Remineralization was absent or sparse in some locations (between open arrowheads). (**D)** A 4-month-old specimen retrieved from the polyacrylic acid- and PVPA-containing SBF showing more extensive but incomplete remineralization of the acid-etched dentin. The original demineralization front was difficult to be discerned (arrow). (**E)** A high-magnification view of Fig. 4D. Intrafibrillar remineralization of a collagen fibril could be seen in an incompletely remineralized region (arrow). Generic abbreviations: Dd, demineralized dentin; Rd, remineralized dentin; Md, naturally mineralized dentin; Ep, epoxy resin; T, dentinal tubule.

Mount GJ (1998). Clinical performance of glass-ionomers. *Biomaterials* 19:573-579.

Naasan MA, Watson TF (1998). Conventional glass ionomers as posterior restorations. A status report for the *American Journal of Dentistry. Am J Dent* 11:36-45.

Ngo HC, Mount G, McIntyre J, Tuisuva J, Von Doussa RJ (2006). Chemical exchange between glass-ionomer restorations and residual carious dentine in permanent molars: an *in vivo* study. *J Dent* 34:608-613.

Niederberger M, Cölfen H (2006). Oriented attachment and mesocrystals: non-classical crystallization mechanisms based on nanoparticle assembly. *Phys Chem Chem Phys* 8:3271-3287.

Pietak AM, Reid JW, Stott MJ, Sayer M (2007). Silicon substitution in the calcium phosphate bioceramics. *Biomaterials* 28: 4023-4032.

Saito T, Toyooka H, Ito S, Crenshaw MA (2003). *In vitro* study of remineralization of dentin: effects of ions on mineral induction by decalcified dentin matrix. *Caries Res* 37:445-449.

Tay FR, Pashley DH (2008). Guided tissue remineralisation of partially demineralised human dentine. *Biomaterials* 29:1127-1137.

Ten Bosch JJ, Angmar-Månsson B (1991). A review of quantitative methods for studies of mineral content of intra-oral caries lesions. *J Dent Res* 70:2-14.

ten Cate JM (2001). Remineralization of caries lesions extending into dentin. *J Dent Res* 80:1407-1411.

Traub W, Arad T, Weiner S (1989). Three-dimensional ordered distribution of crystals in turkey tendon collagen fibers. *Proc Natl Acad Sci USA* 86:9822-9826.

Wang L, Nancollas GH (2009). Pathways to biomineralization and biodemineralization of calcium phosphates: the thermodynamic and kinetic controls. *Dalton Trans* 15:2665-2672.

Wilson AD, Prosser HJ, Powis DM (1983). Mechanism of adhesion of polyelectrolyte cements to hydroxyapatite. *J Dent Res* 62:590-592.

Yoshida Y, Van Meerbeek B, Nakayama Y, Snauwaert J, Hellemans L, Lambrechts P, *et al*. (2000). Evidence of chemical bonding at biomaterial-hard tissue interfaces. *J Dent Res* 79:709-714.

Zavgorodniy AV, Rohanizadeh R, Swain MV (2008). Ultrastructure of dentine carious lesions. *Arch Oral Biol* 53:124-132.

Zhang L, Webster TJ (2009). Nanotechnology and nanomaterials: promises for improved tissue regeneration. *Nano Today* 4:66-80.